JOURNAL OF GUIDANCE, CONTROL, AND DYNAMICS
Vol. 19, No. 5, September–October 1996

Robust Digital Autopilot Design for Spacecraft Equipped with Pulse-Operated Thrusters

Sam W. Thurman*
Jet Propulsion Laboratory, California Institute of Technology, Pasadena, California 91109
and
Henryk Flashner†
University of Southern California, Los Angeles, California 90089

The analysis and design of attitude control systems for spacecraft employing pulse-operated (on–off) thrusters is usually accomplished through a combination of modeling approximations and empirical techniques. A new thruster pulse-modulation theory for pointing and tracking applications is developed from nonlinear control theory. This theory provides the framework for an autopilot suitable for use in digital computers whose performance and robustness properties are characterized analytically, in the design process. Given bounds on the anticipated dynamical modeling errors and sensor errors, it is shown that design specifications can be established and acceptable performance ensured in the presence of these error sources. Spacecraft with time-varying inertia properties can be accommodated, as well as clustered thruster configurations that provide multiple discrete torque levels about one or more spacecraft axes. A realistic application of the theory is illustrated via detailed computer simulation of a digital autopilot designed for midcourse guidance of a hypothetical interplanetary spacecraft.

Introduction

THE analysis and design of three-axis attitude control systems for spacecraft present a challenging problem because of the nonlinear nature of their dynamics. Even in circumstances where linear approximations are valid, the use of pulse-operated (on–off) thrusters for actuation results in systems that are inherently nonlinear. One of the earliest and most widely used design approaches in this case is to assume that the equations of motion are uncoupled, a reasonable approximation for small rotation rates, and employ phase-plane analysis techniques to establish empirical switching curves[1] or to develop control laws that modulate thruster pulse width or frequency to obtain a quasiproportional response.[2] Phase-plane techniques also permit an approximate assessment of limit cycle behavior and the effects of disturbance torques and sensor noise.[1–4] This approach has been used to develop the attitude control systems of space vehicles as diverse as the Apollo spacecraft,[5,6] the Viking Mars lander,[7] and the Space Shuttle.[8] Sophisticated computer simulations were developed and used extensively in the design of these vehicles to validate the approximations employed.

In missions requiring slewing over large angles, Euler's rotation theorem, which specifies that any attitude change of a rigid body can be accomplished by a rotation about an axis fixed with respect to both the vehicle and inertial space, provides a useful and efficient basis for performing these maneuvers. The dynamical coupling inherent in this approach has previously been dealt with in several different ways, such as slewing at small rotation rates to minimize coupling effects,[8] open-loop implementation of a precomputed angular acceleration profile,[9] and the use of feedback linearization to transform the original nonlinear system into an equivalent linear system to which linear control theory can be applied.[10–14] In the feedback linearization schemes discussed in the literature, the control law obtained is a continuously time-varying function. To mechanize this type of control law using pulse-operated thrusters, a second design problem must be solved, that of developing a firing logic that implements the desired torque commands with acceptable accuracy.

In this paper a new class of pulse-mode controllers is developed for pointing and tracking applications, using a modified Euler rotation technique to align the spacecraft with a commanded attitude or attitude profile. These controllers are designed to cause the complete closed-loop system, not just the torque profile produced by the thrusters, to approximate a specified quasilinear system. The important question of robustness is addressed directly: given upper bounds on the sources of modeling error (thrust level variations, center of mass and moment of inertia calibration errors, attitude sensing errors, etc.), design specifications can be established such that the desired performance is ensured in the presence of these error sources. This approach is derived from robust control techniques based on Lyapunov stability theory originated by Corless[15] and Leitmann,[16] which have also been used by the authors for guidance applications.[17] Similar techniques, such as sliding mode control, are described by Utkin[18] and Slotine and Li.[19] Unlike previous approaches based on Lyapunov theory,[11–14] this new approach provides a comprehensive evaluation of robustness properties, and allows for analytical characterization of transient error dynamics, limit cycle deadband, and the effects of attitude and rate estimation errors.

Some spacecraft are equipped with multiple thrusters configured such that two or even three discrete torque levels can be applied to one or more body axes (the Space Shuttle is one example). In addition, the attitude control function on most modern spacecraft is performed by an autopilot implemented as a sampled data system. Using the pulse-modulation theory outlined, the framework of an autopilot suitable for use in digital computers is developed, which is applicable to spacecraft with fixed or time-varying inertia properties and to thruster configurations providing single or multiple torque levels. Inputs can be specified as a commanded attitude or a commanded attitude and rate profile. It is shown that the effect of sampling rate on performance can be assessed within the same analytical framework used to evaluate robustness and performance properties.

Problem Definition

The equations describing the rotational motion of a rigid body are well documented in texts such as those by Hughes[20] and Wertz.[21] These equations can be subdivided into two sets, the dynamical equations relating the rate of change of angular momentum to the applied torque, and a set of kinematic equations that relate some parameterization of the attitude to the angular velocity of the body. For

Received Feb. 27, 1995; revision received May 1, 1996; accepted for publication May 3, 1996.

*Member, Technical Staff, Flight Systems Engineering Section, Systems Division, 4800 Oak Grove Drive. Senior Member AIAA.

†Associate Professor, Departments of Mechanical and Aerospace Engineering, University Park. Member AIAA.

spacecraft equipped with mass expulsion devices such as thrusters, the moments of inertia of the vehicle will be time varying in addition to the angular momentum vector.

Designating the inertia tensor as $\boldsymbol{J}$, the angular velocity vector as $\boldsymbol{\omega}$, and the applied torque vector as $\boldsymbol{m}$, the dynamical equations of a rigid spacecraft expressed in a body-fixed frame are as follows:

$$\boldsymbol{J}\dot{\boldsymbol{\omega}} = \boldsymbol{m} - \dot{\boldsymbol{J}}\,\boldsymbol{\omega} - \boldsymbol{\omega} \times \boldsymbol{J}\boldsymbol{\omega} - \sum_{i=1}^{M} \dot{m}_i[\boldsymbol{l}_i \times (\boldsymbol{\omega} \times \boldsymbol{l}_i)] \tag{1}$$

In Eq. (1), $\dot{m}_i$ is the propellant mass flow rate of the ith thruster ($\dot{m}_i > 0$ by convention) and the vector $\boldsymbol{l}_i$ is the position of the ith thruster with respect to the center of mass of the spacecraft. The terms in this equation as a result of the rate of change of inertia and propellant expulsion are usually small compared with the other terms, but can be significant during large propulsive maneuvers. The applied torque vector $\boldsymbol{m}$ is

$$\boldsymbol{m} = \sum_{i=1}^{N} \boldsymbol{l}_i \times \boldsymbol{f}_i \tag{2}$$

In Eq. (2), the vector $\boldsymbol{l}_i$ has the same meaning as in Eq. (1), whereas $\boldsymbol{f}_i$ represents the thrust vector of the ith thruster.

The thrust profile of a representative thruster firing is shown in Fig. 1. As suggested by this illustration, some thrusters can exhibit a noticeable departure from an ideal square wave profile. The ignition and termination commands are each followed by a delay resulting from the electrical and mechanical operation of the propellant valves, and a thrust buildup or decay period, respectively. Typical values for these delay times and buildup and decay periods range from just a few milliseconds to several hundred milliseconds, depending on the size and type of thruster. The steady-state thrust level also varies roughly 1–20% between successive firings, depending on the firing period and type of thruster, with the greatest variation occurring when using very short or very long pulses.

For attitude parameterization an Euler symmetric parameter, or quaternion, representation is one of the most useful for attitude control systems and will be employed herein. The attitude quaternion, which consists of a three-element vector part and a scalar part, is specified as follows:

$$\boldsymbol{q} = [\sin(\varphi/2)\boldsymbol{\lambda}, \cos(\varphi/2)] \tag{3}$$

In Eq. (3), $\boldsymbol{\lambda}$ is a unit vector about which a rotation through the angle φ will move the designated spacecraft body-fixed coordinate frame from a nonrotating reference frame into its current orientation. The evolution of the quaternion is governed by the following differential equation:

$$\dot{\boldsymbol{q}} = \tfrac{1}{2}\boldsymbol{\Omega}\boldsymbol{q} \tag{4}$$

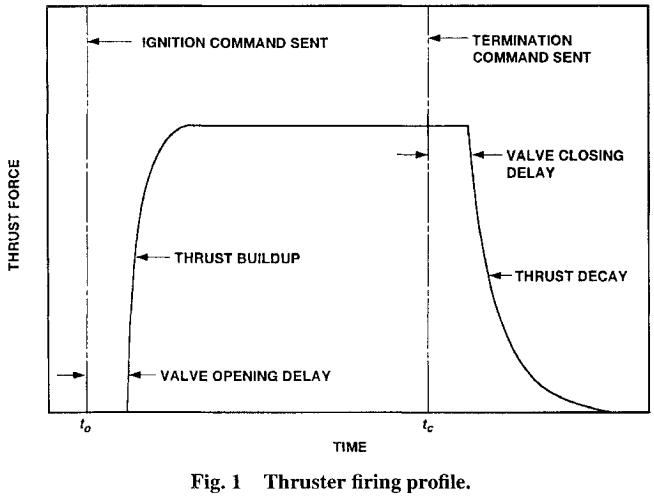

Fig. 1 Thruster firing profile.

where

$$\boldsymbol{\Omega} = \begin{bmatrix} 0 & \omega_3 & -\omega_2 & \omega_1 \\ -\omega_3 & 0 & \omega_1 & \omega_2 \\ \omega_2 & -\omega_1 & 0 & \omega_3 \\ -\omega_1 & -\omega_2 & -\omega_3 & 0 \end{bmatrix} \tag{5}$$

In Eq. (5), ω_1, ω_2, and ω_3 are the angular velocity components expressed in the designated body-fixed frame, i.e., $\boldsymbol{\omega} = [\omega_1\ \omega_2\ \omega_3]^T$. Equation (4) uses a column vector representation of the quaternion $\boldsymbol{q}$, such that $\boldsymbol{q} = [q_1\ q_2\ q_3\ q_4]^T$, where the first three elements (q_1, q_2, q_3) constitute the vector part of the quaternion and the fourth element (q_4) is the scalar part.

With this representation, attitude commands are specified as a quaternion, designated $\boldsymbol{q}_c$, or a time history $\boldsymbol{q}_c(t)$ and its associated rate history $\boldsymbol{\omega}_c(t)$ corresponding to an attitude profile. The error quaternion, designated $\Delta\boldsymbol{q}$, representing a unique rotation axis and angle needed to move the spacecraft from its current attitude, specified by $\boldsymbol{q}$, into alignment with the commanded attitude $\boldsymbol{q}_c$, can be computed using quaternion multiplication:

$$\Delta\boldsymbol{q} = \boldsymbol{q}^{-1}\boldsymbol{q}_c \tag{6}$$

The inverse quaternion $\boldsymbol{q}^{-1}$ is defined as follows:

$$\boldsymbol{q}^{-1} = [-\sin(\varphi/2)\boldsymbol{\lambda}, \cos(\varphi/2)] \tag{7}$$

The resulting error quaternion can be written as

$$\Delta\boldsymbol{q} = [\sin(\Delta\varphi/2)\boldsymbol{e}, \cos(\Delta\varphi/2)] \tag{8}$$

The unit vector $\boldsymbol{e}$ in Eq. (8) represents the axis about which a rotation of angle $\Delta\varphi$ will bring the vehicle into alignment with the commanded attitude or point along an attitude profile. A controller employing the quantities $\Delta\boldsymbol{q}$ and $\Delta\boldsymbol{\omega}$, where $\Delta\boldsymbol{\omega} = \boldsymbol{\omega} - \boldsymbol{\omega}_c$, is sought that is compatible with the restrictions associated with pulse-operated thrusters, yet still achieves acceptable performance.

Pulse-Modulation Control Theory

The proposed pulse-modulation technique consists of equations defining the commanded torque and the thruster firing logic. It is intended for spacecraft with thruster configurations that can apply torque about each axis of a designated body-fixed frame; these torques are not required to be mutually orthogonal. Two different pulse-mode controllers are presented, one that contains no model parameters and the other containing model-dependent feedforward terms, analogous to the continuous-time control laws presented by Wen and Kreutz-Delgado[13] and Weiss.[14]

Commanded Torque Formulation

A general form for the commanded torque vector $\boldsymbol{m}_c$ that encompasses both the model-independent and model-dependent cases is as follows:

$$\boldsymbol{m}_c = \hat{\boldsymbol{u}}(\Delta\hat{\boldsymbol{\Phi}}, \Delta\hat{\boldsymbol{\omega}}) + \boldsymbol{K}_\epsilon(\bar{\boldsymbol{J}}, \bar{\boldsymbol{m}}_i, \bar{\boldsymbol{l}}_i, \hat{\boldsymbol{\omega}}, \dot{\boldsymbol{\omega}}_c)\boldsymbol{n}[(1/\epsilon)\hat{\boldsymbol{v}}(\Delta\hat{\boldsymbol{\Phi}}, \Delta\hat{\boldsymbol{\omega}}] + \boldsymbol{c}(\bar{\boldsymbol{J}}, \bar{\boldsymbol{m}}_i, \bar{\boldsymbol{l}}_i, \hat{\boldsymbol{\omega}}, \dot{\boldsymbol{\omega}}_c) \tag{9}$$

where

$$\Delta\hat{\boldsymbol{\Phi}} = \Delta\hat{\varphi}\hat{\boldsymbol{e}} \tag{10}$$

The quantities in Eqs. (9) and (10) can be time varying unless specifically stated otherwise. The first two terms of Eq. (9) are intended to null attitude and rate tracking errors, whereas the third term represents any desired model compensation terms, designed to reduce or eliminate nonlinear elements of the dynamical equations, and feedforward terms to aid in following a commanded attitude and rate profile. The vectors $\Delta\boldsymbol{\Phi}$, $\Delta\boldsymbol{\omega}$, and $\boldsymbol{\omega}$ are denoted with carets to indicate that only estimates of these parameters, derived from sensor data onboard the spacecraft, are used in the computations. The quantities $\boldsymbol{J}$, $\dot{m}_i$, and $\boldsymbol{l}_i$ are denoted with overbar symbols to show that inexact estimates of these parameters are also used, the difference being that these quantities are often not estimated from sensor data (notable exceptions exist, such as adaptive controllers that attempt

to estimate $\boldsymbol{J}$ during their operation[13]); a priori estimates or values computed from some nominal model are used instead. The estimated attitude error angle and rotation axis appearing in Eq. (10) are obtained from an estimate of the quaternion $\Delta\boldsymbol{q}$ defined in Eq. (8):

$$\Delta\hat{\varphi} = 2\cos^{-1}\Delta\hat{q}_4 \tag{11}$$

$$\hat{\boldsymbol{e}} = \left(1 - \Delta\hat{q}_4^2\right)^{\frac{1}{2}}[\Delta\hat{q}_1 \quad \Delta\hat{q}_2 \quad \Delta\hat{q}_3]^T \tag{12}$$

In Eq. (12), the vector $\boldsymbol{e}$ is defined such that the rotation required to bring the spacecraft into alignment with the commanded attitude is always positive in a right-handed sense ($\Delta\varphi > 0$).

The vector functions $\hat{\boldsymbol{u}}$ and $\hat{\boldsymbol{v}}$ appearing in Eq. (9) consist of proportional and derivative feedback terms with the following form:

$$\hat{\boldsymbol{u}} = \boldsymbol{K}_P\Delta\hat{\boldsymbol{\Phi}} - \boldsymbol{K}_D\Delta\hat{\boldsymbol{\omega}} \tag{13}$$

$$\hat{\boldsymbol{v}} = k_P\Delta\hat{\boldsymbol{\Phi}} - k_D\Delta\hat{\boldsymbol{\omega}} \tag{14}$$

As in Eq. (9), $\boldsymbol{u}$ and $\boldsymbol{v}$ are denoted with carets in Eqs. (13) and (14), signifying that they are determined from estimates of $\Delta\boldsymbol{\Phi}$ and $\Delta\boldsymbol{\omega}$, rather than their true values, when computing the commanded torque. In Eq. (13), $\boldsymbol{K}_P$ and $\boldsymbol{K}_D$ are constant 3×3 gain matrices, whereas k_P and k_D in Eq. (14) are positive, constant scalars. The matrices $\boldsymbol{K}_P$ and $\boldsymbol{K}_D$ are symmetric and positive definite, and must satisfy the following relationships with k_P and k_D:

$$\frac{\|\boldsymbol{K}_P\Delta\boldsymbol{\Phi}\|}{\bar{\sigma}(\boldsymbol{J})} \geq k_P\|\Delta\boldsymbol{\Phi}\| \tag{15}$$

$$\frac{\|\boldsymbol{K}_D\Delta\boldsymbol{\omega}\|}{\bar{\sigma}(\boldsymbol{J})} \geq k_D\|\Delta\boldsymbol{\omega}\| \tag{16}$$

The double lines in Eqs. (15) and (16) signify the Euclidean norm of the bracketed vector, whereas $\bar{\sigma}(\boldsymbol{J})$ represents an upper bound on the largest eigenvalue of the inertia tensor $\boldsymbol{J}$. These equations require the induced norm of $\boldsymbol{K}_P$ and $\boldsymbol{K}_D$ to be large enough such that the commanded torque specified by $\boldsymbol{u}$ delivers, at a minimum, the angular acceleration specified by the vector $\boldsymbol{v}$.

The 3×3 matrix $\boldsymbol{K}_\epsilon$ and the vector function $\boldsymbol{n}$ appearing in Eq. (9) are designed to simultaneously compensate for known torque implementation errors as a result of the use of discrete thruster firings, and unknown or uncompensated dynamical effects; the requirements they must satisfy are described in further detail subsequently. The scalar parameter ϵ ultimately determines the control accuracy that can be achieved, and will also be discussed subsequently.

The third and final term appearing in Eq. (9) is the vector function $\boldsymbol{c}$, containing model compensation and feedforward terms that may be used to improve performance and efficiency in some scenarios. The most comprehensive expression that can be employed here is as follows:

$$\boldsymbol{c} = \hat{\boldsymbol{\omega}} \times \bar{\boldsymbol{J}}\,\hat{\boldsymbol{\omega}} + \dot{\bar{\boldsymbol{J}}}\,\hat{\boldsymbol{\omega}} + \sum_{i=1}^{M} \bar{m}_i[\bar{\boldsymbol{l}}_i \times (\hat{\boldsymbol{\omega}} \times \bar{\boldsymbol{l}}_i)] \tag{17}$$

The first three terms of Eq. (17) will ideally cancel the gyroscopic and mass expulsion terms of Eq. (1). The fourth term is a feedforward torque profile to aid in tracking a commanded attitude and rate profile, if one is desired. For precision tracking applications, the terms in Eq. (17) are not always necessary; usually only the gyroscopic term and the input torque profile are needed.

Pulse-Mode Controller Dynamics

The thruster firing logic employed herein is to select a thruster combination at each command interval that delivers the torque vector most closely matching the commanded torque $\boldsymbol{m}_c$ given by Eq. (9). Equation (9) is structured such that straightforward application of this firing logic yields satisfactory performance. The actual applied torque vector $\boldsymbol{m}$ is written as

$$\boldsymbol{m} = \boldsymbol{m}_c + \Delta\boldsymbol{m} + \delta\boldsymbol{m} \tag{18}$$

In Eq. (18), the vector $\Delta\boldsymbol{m}$ is equal to the difference between $\boldsymbol{m}_c$ and the nearest torque value that can nominally be obtained, whereas the vector $\delta\boldsymbol{m}$ represents torque implementation errors resulting from thrust level variations, thruster misalignment, calibration errors, etc. Further characterization of $\delta\boldsymbol{m}$ requires specific knowledge of thruster specifications and their configurations.

Substituting Eq. (18) into Eq. (1) and making use of Eqs. (9), (13), (14), and (17) yields the following equation of motion for the closed-loop system:

$$\Delta\dot{\boldsymbol{\omega}} = \boldsymbol{J}^{-1}\{\boldsymbol{K}_P\Delta\boldsymbol{\Phi} - \boldsymbol{K}_D\Delta\boldsymbol{\omega} + \boldsymbol{K}_\epsilon\boldsymbol{n}[(1/\epsilon)(k_P\Delta\boldsymbol{\Phi} - k_D\Delta\boldsymbol{\omega} + \delta\boldsymbol{v})] + \boldsymbol{h}\} \tag{19}$$

where

$$\boldsymbol{h} = \boldsymbol{c} - \boldsymbol{\omega} \times \boldsymbol{J}\boldsymbol{\omega} - \dot{\boldsymbol{J}}\,\boldsymbol{\omega} - \sum_{i=1}^{M} \dot{m}_i[\boldsymbol{l}_i \times (\boldsymbol{\omega} \times \boldsymbol{l}_i)] - \boldsymbol{J}\dot{\boldsymbol{\omega}}_c + \Delta\boldsymbol{m} + \delta\boldsymbol{m} + \delta\boldsymbol{u} \tag{20}$$

For simplicity in Eq. (19), the arguments of $\boldsymbol{K}_\epsilon$ are no longer shown. The vectors $\delta\boldsymbol{u}$ and $\delta\boldsymbol{v}$ in Eqs. (19) and (20) represent erroneous commands induced by attitude and rate sensing errors:

$$\delta\boldsymbol{u} = \boldsymbol{K}_P\delta\boldsymbol{\Phi} - \boldsymbol{K}_D\delta\boldsymbol{\omega} \tag{21}$$

$$\delta\boldsymbol{v} = k_P\delta\boldsymbol{\Phi} - k_D\delta\boldsymbol{\omega} \tag{22}$$

In Eqs. (21) and (22), $\delta\boldsymbol{\Phi}$ and $\delta\boldsymbol{\omega}$ represent attitude and rate estimation errors, respectively.

The properties of the matrix $\boldsymbol{K}_\epsilon$ and the vector function $\boldsymbol{n}$ of Eq. (9) will now be addressed. The matrix $\boldsymbol{K}_\epsilon$ is symmetric and positive definite; it must also satisfy the following constraint:

$$\|\boldsymbol{K}_\epsilon\boldsymbol{n}\|/\bar{\sigma}(\boldsymbol{J}) \geq k_\epsilon\|\boldsymbol{n}\| \tag{23}$$

where

$$k_\epsilon \geq \|\boldsymbol{h}\|/\underline{\sigma}(\boldsymbol{J}) \tag{24}$$

The function k_ϵ appearing in Eqs. (23) and (24) is designed to ensure that the commanded angular acceleration because of the term $\boldsymbol{J}^{-1}\boldsymbol{K}_\epsilon\boldsymbol{n}$ in Eq. (19) will be larger than any unmodeled disturbances and uncompensated angular accelerations represented by $\boldsymbol{J}^{-1}\boldsymbol{h}$. In Eqs. (23) and (24), $\bar{\sigma}(\boldsymbol{J})$ and $\underline{\sigma}(\boldsymbol{J})$ represent upper and lower bounds on the eigenvalues of the inertia tensor $\boldsymbol{J}$, respectively. If needed, k_ϵ can be specified in terms of model parameters such as $\bar{\boldsymbol{J}}$, $\hat{\boldsymbol{\omega}}$, $\dot{\boldsymbol{\omega}}_c$, etc., to track dynamical variations in the vector $\boldsymbol{J}^{-1}\boldsymbol{h}$, or k_ϵ can be a constant representing a global bound. Note that for a model-independent controller, in which the function $\boldsymbol{c}$ from Eq. (17) is set to zero, the vector $\boldsymbol{h}$ of Eq. (20) will be larger than it would be if model compensation was employed, imposing a greater requirement on k_ϵ. The function $\boldsymbol{n}$ can be any function with the following properties.

Condition 1:

$$\|\boldsymbol{v}\|\boldsymbol{n}(\epsilon, \boldsymbol{v}) = \|\boldsymbol{n}(\epsilon, \boldsymbol{v})\|\boldsymbol{v} \tag{25a}$$

Condition 2:

$$\|\boldsymbol{n}(\epsilon, \boldsymbol{v}) \geq 1 - \epsilon/\|\boldsymbol{v}\|; \qquad \|\boldsymbol{v}\| > \epsilon \tag{25b}$$

Stability Analysis

The stability of the system defined by Eqs. (19–22) will be evaluated using Lyapunov theory.[15–20] A Lyapunov function candidate is sought that shows that within the domain of $\Delta\boldsymbol{\Phi}$ and $\Delta\boldsymbol{\omega}$ all possible trajectories are globally, uniformly, and exponentially convergent to within a small region of radius b around the origin ($\Delta\boldsymbol{\Phi} = \boldsymbol{0}$, $\Delta\boldsymbol{\omega} = \boldsymbol{0}$). Designating the vector $\boldsymbol{x} = [\Delta\boldsymbol{\Phi} \ \Delta\boldsymbol{\omega}]^T$, the system is said to be exponentially convergent with rate α to the desired vicinity around the origin if, for some positive constant β, the following inequality is satisfied:

$$\|\boldsymbol{x}(t)\| \leq b + \beta\|\boldsymbol{x}(t_0)\| \exp[-\alpha(t - t_0)]; \qquad t \geq t_0 \tag{26}$$

The proposed Lyapunov function candidate, designated $V(\boldsymbol{x})$, is

$$V(\boldsymbol{x}) = \frac{1}{2}\boldsymbol{x}^T\boldsymbol{P}\boldsymbol{x} = \frac{1}{2}[\Delta\boldsymbol{\Phi}^T \quad \Delta\boldsymbol{\omega}^T]\begin{bmatrix} k_L\boldsymbol{I} & -k_P\boldsymbol{I} \\ -k_P\boldsymbol{I} & k_D\boldsymbol{I} \end{bmatrix}\begin{bmatrix} \Delta\boldsymbol{\Phi} \\ \Delta\boldsymbol{\omega} \end{bmatrix} \tag{27}$$

As shown in Eq. (27), the matrix $\boldsymbol{P}$ is composed of four 3×3 submatrices ($\boldsymbol{I}$ is the identity matrix). The parameters k_P and k_D are

defined in Eqs. (15) and (16), respectively; k_L will subsequently be determined such that the required stability criteria are satisfied. For the system to behave according to Eq. (26), $V(\boldsymbol{x})$ must satisfy the following conditions, as shown by Corless.[15]

Condition 1:

$$c_1\|\boldsymbol{x}\|^2 \leq V(\boldsymbol{x}) \leq c_2\|\boldsymbol{x}\|^2; \qquad c_1, c_2 > 0 \tag{28a}$$

Condition 2:

$$\dot{V}(\boldsymbol{x}) \leq -2\alpha[V(\boldsymbol{x}) - V^*]; \qquad V(\boldsymbol{x}) > V^* \tag{28b}$$

Equations (28) represent a set of sufficient, not necessary, conditions. If a Lyapunov function satisfying these conditions is not found, or if for some $V(\boldsymbol{x})$ Eq. (28) is violated for a specific value of $\boldsymbol{x}$, this does not necessarily imply that the origin of the system is unstable.

To satisfy condition 1 of Eq. (28), the matrix $\boldsymbol{P}$ of Eq. (27) must be positive definite. To check condition 2 of Eq. (28), the derivative of $V(\boldsymbol{x})$ is needed; this is obtained using Eqs. (27) and (19):

$$\dot{V} = k_L\Delta\varphi\Delta\dot{\varphi} + k_P\Delta\dot{\varphi}^2 + \left(k_D\Delta\boldsymbol{\omega}^T - k_P\Delta\boldsymbol{\Phi}^T\right)\boldsymbol{J}^{-1}$$
$$\times\{\boldsymbol{K}_P\Delta\boldsymbol{\Phi} - \boldsymbol{K}_D\Delta\boldsymbol{\omega} + \boldsymbol{K}_\epsilon\boldsymbol{n}[(1/\epsilon)\hat{\boldsymbol{v}}] + \boldsymbol{h}\} \tag{29}$$

Using Eqs. (15), (16), (23), and (24), and noting that $\Delta\boldsymbol{\Phi}^T\Delta\boldsymbol{\omega} = \Delta\boldsymbol{\omega}^T\Delta\boldsymbol{\Phi} = -\Delta\varphi\Delta\dot{\varphi}$, Eq. (29) can be shown to satisfy the following inequality:

$$\dot{V} \leq -k_P^2\Delta\varphi^2 + \left(k_P - k_D^2\right)\|\Delta\boldsymbol{\omega}\|^2 + (k_L - 2k_Pk_D)\Delta\varphi\Delta\dot{\varphi}$$
$$-\boldsymbol{v}^T\left\{k_\epsilon\boldsymbol{n}[(1/\epsilon)\hat{\boldsymbol{v}}] + \boldsymbol{J}^{-1}\boldsymbol{h}\right\} \tag{30}$$

In Eq. (30), $\boldsymbol{v}^T = [k_P\Delta\boldsymbol{\Phi}^T + k_D\Delta\boldsymbol{\omega}^T]$. By comparing terms in Eqs. (27) and (30), the following formulas for k_D, k_P, and k_L are obtained that fulfill both conditions of Eq. (28):

$$\begin{bmatrix} k_L & -k_P \\ -k_P & k_D \end{bmatrix} = 2\alpha\begin{bmatrix} 2\alpha^2 & -\alpha \\ -\alpha & 1 \end{bmatrix} \tag{31}$$

Substituting Eq. (31) into Eq. (30) and noting that $\boldsymbol{v} = \hat{\boldsymbol{v}} - \delta\boldsymbol{v}$ leads to the following:

$$\dot{V}(\boldsymbol{x}) \leq -2\alpha[V(\boldsymbol{x}) - (E/2\alpha)] \tag{32}$$

where

$$E = -(\hat{\boldsymbol{v}} - \delta\boldsymbol{v})^T\left\{k_\epsilon\boldsymbol{n}[(1/\epsilon)\hat{\boldsymbol{v}}] + \boldsymbol{J}^{-1}\boldsymbol{h}\right\} \tag{33}$$

By establishing an upper bound on the parameter E of Eq. (33), condition 2 of Eq. (28) is satisfied by choosing $V^* = \bar{E}/2\alpha$, where $\bar{E}$ is the indicated upper bound. Equation (33) can be further characterized using the requirements on the function $\boldsymbol{n}$ given in Eq. (25). Using condition 1 of Eq. (25), further manipulation of Eq. (33) yields the following expression:

$$E \leq \|\hat{\boldsymbol{v}}\|[\|\boldsymbol{h}\|/\underline{\sigma}(\boldsymbol{J}) - k_\epsilon\|\boldsymbol{n}\|] + \|\delta\boldsymbol{v}\|[\|\boldsymbol{h}\|/\underline{\sigma}(\boldsymbol{J}) + k_\epsilon\|\boldsymbol{n}\|] \tag{34}$$

By examining the behavior of the quantities appearing in Eq. (34) for a specific vehicle and application, a suitable value of $\bar{E}$ can be established. Condition 2 of Eq. (25) implies that progressively smaller values of ϵ, an argument of the function $\boldsymbol{n}$, result in correspondingly smaller limits on the magnitude of the first bracketed term of E in Eq. (34); the magnitude of this term approaches zero in the limit as ϵ approaches zero. As would be expected, a decrease in ϵ implies an increase in thruster activity. The practical consequence is a trade between control accuracy and propellant consumption, which is governed by the number and frequency of thruster firings. The second term in Eq. (34) provides an intuitive result, showing that attitude and rate sensing errors, which manifest themselves in $\delta\boldsymbol{v}$, impose a fundamental limit on the smallest value of E than can actually be achieved, independent of the value of ϵ selected.

A Lyapunov function meeting the stated requirements ensures exponential convergence of $\boldsymbol{x}$ to within a neighborhood around the origin defined by $V(\boldsymbol{x}) \leq V^*$ (recall that $V^* = \bar{E}/2\alpha$) (Refs. 22 and 23). Using Eqs. (27), (31), and (32), the following expression is obtained for this region:

$$4\alpha^4\Delta\varphi^2 + 2\alpha^2\Delta\dot{\varphi}^2 + 4\alpha^3\Delta\varphi\Delta\dot{\varphi} \leq \bar{E} \tag{35}$$

Once the state has entered the domain specified by Eq. (35), it will remain there indefinitely. Thus, Eq. (35) can be used to illustrate the limit cycle envelope of the controller graphically, in a manner similar to phase-plane analysis.[23]

Digital Autopilot Design

This section describes the primary considerations in the design of a spacecraft autopilot for digital computer implementation. The pulse-mode control theory, as just presented, implicitly assumes that the parameters needed to compute torque commands are continuously available and that those commands are continuously executed without any computational or mechanical delays. However, the theory is applicable to sampled data systems with proper interpretation.

Design Parameters

In a sampled data system, the command torque expression of Eq. (9) is evaluated at discrete intervals. Using Eqs. (9), (13), (14), and (17), the following expression is obtained:

$$\boldsymbol{m}_c(t_k) = \boldsymbol{K}_P\Delta\hat{\boldsymbol{\Phi}}_k - \boldsymbol{K}_D\Delta\hat{\boldsymbol{\omega}}_k$$
$$+\boldsymbol{K}_\epsilon\boldsymbol{n}[(1/\epsilon)(k_P\Delta\hat{\boldsymbol{\Phi}}_k - k_D\Delta\hat{\omega}_k)] + \boldsymbol{c}_k \tag{36}$$

In Eq. (36) the subscript k implies the value of the indicated quantity at time t_k. A useful form for the function $\boldsymbol{n}$ satisfying the conditions of Eq. (25) that mimics the behavior of the thrusters is as follows:

$$\begin{aligned} \boldsymbol{n}(\epsilon, \hat{\boldsymbol{v}}) &= \boldsymbol{0}; & \|\hat{\boldsymbol{v}}\| &< \epsilon \\ \boldsymbol{n}(\epsilon, \hat{\boldsymbol{v}}) &= \hat{\boldsymbol{v}}/\|\hat{\boldsymbol{v}}\|; & \|\hat{\boldsymbol{v}}\| &\geq \epsilon \end{aligned} \tag{37}$$

The key design parameters to be chosen are the rate of convergence α, which determines the values of the feedback gains k_P and k_D given in Eq. (31); the parameter ϵ, which sets the thruster firing deadband in Eq. (37); and the interval between command updates, designated T. When designing a model-independent autopilot for a spacecraft that can apply only a single torque level to each axis, a simpler version of Eq. (36) can be used, by eliminating the first, second, and fourth terms. These terms are then treated as part of the vector $\boldsymbol{h}$ of Eq. (20), along with all other uncompensated or unmodeled dynamical terms. As long as $\boldsymbol{K}_\epsilon$ in Eq. (36) satisfies Eqs. (23) and (24), the exponential stability criteria of Eq. (28) hold, with $\boldsymbol{m}_c(t_k)$ determined solely by the third term of Eq. (36).

Thruster valve characteristics limit the smallest pulse width for which reliable operation is assured. This effectively sets the smallest usable value of T, and limits control precision to levels commensurate with the angular position and rate changes induced by minimum impulse thruster firings. For zero-order sample-and-hold systems, the same logic still applies for larger values of T, in that the attitude and rate changes resulting from a thruster pulse of T seconds limit the achievable precision. In one sense a minimum pulse width is beneficial, as it incorporates hysteresis into the digital controller that prevents chattering of the thruster valves. For values of T that are small relative to the frequency range of the spacecraft dynamics, the following expressions are useful:

$$\begin{aligned} |\Delta\dot{\varphi}|_{\min} &\approx [m/\underline{\sigma}(\boldsymbol{J})]T \\ |\Delta\varphi|_{\min} &\approx (T/2)|\Delta\dot{\varphi}|_{\min} \end{aligned} \tag{38}$$

In Eq. (38), $\boldsymbol{m}$ represents the torque capability of the spacecraft; $\underline{\sigma}(\boldsymbol{J})$ has the same meaning as in Eq. (24). Equation (38) provides approximate upper bounds on the minimum values of $\Delta\varphi$ and $\Delta\dot{\varphi}$ that can be achieved for a given T, independent of other error sources, such as high-frequency attitude sensor noise, that can also influence the choice of ϵ. The bounds in Eq. (38) provide a guideline for an approximate lower bound on ϵ that will ensure a sufficiently large thruster firing deadband:

$$\epsilon > k_P|\Delta\varphi|_{\min} + k_D|\Delta\dot{\varphi}|_{\min} \tag{39}$$

In addition to sampling rate considerations, time delays between the sampling of attitude sensors and the implementation of thruster firing commands must be considered. This error source can be interpreted as a modeling error in Eqs. (18) and (20); its effect will be addressed further.

Performance Specifications

In the transient phase of operation, a pulse-mode controller based on Eqs. (36) and (37) forces the closed-loop system to mimic the response of a linear proportional-plus-derivative controller:

$$\Delta\ddot{\varphi} + k_D\Delta\dot{\varphi} + k_P\Delta\varphi \approx 0 \tag{40}$$

Overall, Eq. (40) yields the most accurate approximation of transient behavior in rest-to-rest slew maneuvers, in which the angular velocity vector of the spacecraft is ideally parallel with the Euler rotation axis [note that the use of Eq. (40) as an analytical tool admits negative values of the attitude error angle $\Delta\varphi$]. The values of k_P and k_D given in Eq. (31) in terms of the convergence rate α yield the following damping ratio ζ and natural frequency f_n of the closed-loop system[23]:

$$\zeta \approx 0.707 \qquad f_n \approx (1/\sqrt{2}\pi)\alpha \tag{41}$$

For the indicated damping ratio, the natural frequency of the system is also equal to its -3-dB bandwidth; hence, the bandwidth is immediately determined by the value of α selected.

Once the spacecraft's attitude state has entered the region specified by Eq. (35), it will exhibit some type of limit cycle behavior thereafter, with the envelope of this region established by the parameter E of Eqs. (33) and (34). For slew maneuvers in which the terminal value of the commanded angular velocity ω_c is zero, the following approximation is useful[23]:

$$\bar{E} \approx (\epsilon + \xi)(\epsilon + \overline{\delta v}) \tag{42}$$

Equation (42) incorporates approximate upper bounds (just prior to a thruster firing) on the vector $\hat{v}$ of Eq. (14), the disturbance vector $\boldsymbol{h}$ of Eq. (20), and the erroneous angular acceleration commands of Eq. (22), designated $\overline{\delta v}$. The parameter ξ bounds thrust implementation errors in Eq. (20) resulting from the interval between command computations (T) and any time delays present in the system; in most modern spacecraft control systems, ξ is small compared with the other parameters in Eq. (42). Using Eq. (42), an accurate estimate of the limit cycle regime can be obtained from Eq. (35).

Midcourse Guidance Computer Simulation

This section describes a digital autopilot for midcourse guidance of an interplanetary spacecraft. In this scenario, a hypothetical soft lander approaching the planet Mars performs a late propulsive maneuver to remove residual targeting errors about 30 min prior to atmospheric entry, descent, and landing. This vehicle is similar to the Mars Pathfinder spacecraft,[24] which in actual operation executes maneuvers via ground-based commands, rather than onboard control.

Spacecraft Description

The spacecraft configuration in interplanetary flight is shown in Fig. 2. Specific configuration data are provided in Table 1. The lander is carried to Mars inside an entry vehicle attached to a cruise stage. The cruise stage is equipped with sun sensors and a star tracker for attitude determination, eight thrusters for attitude control and midcourse propulsion, and a solar array for power generation. Note that the plane containing the roll thrusters is offset from the spacecraft's center of mass about 10 cm. The thruster configuration, although efficient, provides the capability for coupled torques only about the roll axis; pitch and yaw thruster firings yield both torques and translational velocity changes. The lander carries a strapdown inertial measurement unit (IMU), which is used to perform inertial navigation during midcourse maneuvers and the terminal descent phase.

A high-level block diagram of the spacecraft's midcourse guidance system is shown in Fig. 3. The key parameters of the digital autopilot are given in Table 2. A velocity-to-be-gained method is used for guidance,[25] in which the spacecraft maneuvers itself to null the velocity-to-be-gained vector, representing the difference between the velocity required to achieve the proper atmospheric entry

Table 1 Spacecraft configuration data

Parameter	Nominal value	RMS (1σ) variation
Initial mass		
Spacecraft (dry), kg	420.0	0.5%
Propellant/oxidizer, kg	30.0	2.0%
Initial moments of inertia		
Yaw (z axis), kg-m^2	120.0	2.0%
Pitch (y axis), kg-m^2	115.0	2.0%
Roll (x axis), kg-m^2	145.0	2.0%
Cross products, kg-m^2	<5.0	—
Center of mass offset, cm	0.0	1.0
Thruster specifications		
Thrust level, N	4.45	3.0%
Min pulse width, ms	20	—
Rise time, ms	2.0	—
Decay time, ms	3.0	—
Valve open/close delay, ms	3.0	—
Max acceleration, m/s^2	0.04	2.5%
Max angular acceleration, rad/s^2	0.067	3.6%

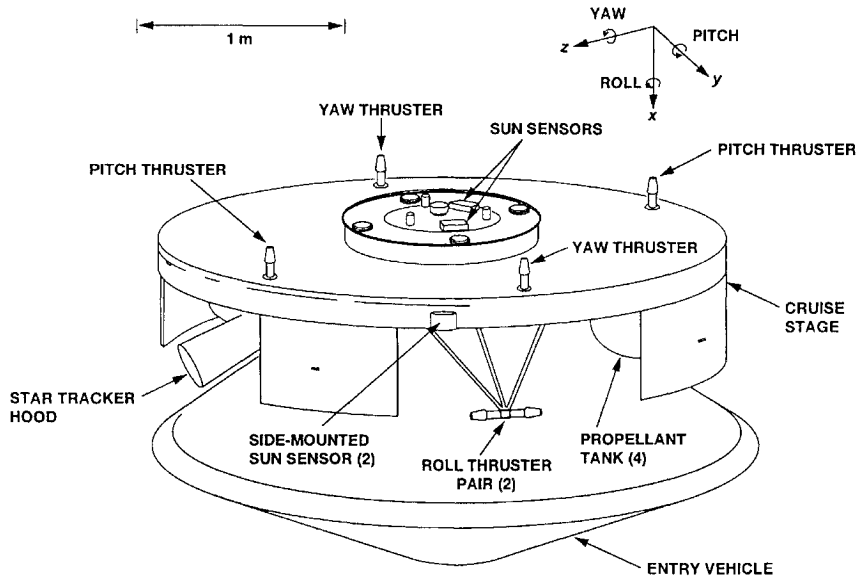

Fig. 2 Spacecraft configuration.

conditions and the velocity indicated by the inertial navigation system. At each command interval (the subscript k in Fig. 3 signifies the value of the indicated parameter at time t_k), the guidance law supplies the autopilot with the velocity-to-be-gained vector. The spacecraft is commanded to assume an attitude that will align the thrust axis with the velocity-to-be-gained vector; this logic is used to derive the commanded attitude quaternion shown in Fig. 3. These quantities, along with estimates of the current attitude quaternion and angular velocity vector obtained from the navigation system, are used to determine the command torque vector.

The autopilot employs a simple model-independent pulse-mode controller. The commanded torque is computed using the third term of Eq. (36) and Eq. (37), as described earlier (see Fig. 3). The matrix $\boldsymbol{K}_\epsilon$ of Eq. (36) is diagonal, with the values on the diagonal being the nominal torque generated about the x, y, and z spacecraft body axes, respectively, by the appropriate thruster firings. These values are labeled m_x, m_y, and m_z in Table 2. At each command interval, the autopilot issues commands to the thruster valves only when a change in the state of a given thruster is needed. When the guidance system senses that the spacecraft is within the limit cycle envelope of Eq. (35), the thrusters are used to carry out velocity changes. During these periods, certain thrusters may be turned off momentarily, when torque commands for attitude maintenance are issued.

The thruster characteristics given in Table 1 are representative of modern bipropellant engines for small-spacecraft propulsion.[26] The error model used to represent the inertial navigation system is summarized in Table 3. The IMU contains three ring-laser gyroscopes and three pendulous accelerometers; its performance is representative of the strapdown IMUs carried by the Clementine spacecraft.[27] The error model components in Table 3 are based on established modeling techniques for these instruments.[28] The navigation system is initialized with ground-based estimates of the spacecraft's position and velocity vectors relative to Mars[29]; the initial attitude quaternion is established by an alignment process performed onboard the spacecraft using its attitude sensors. The bias errors of the gyroscopes and accelerometers are also calibrated during the alignment process.

Table 2 Digital autopilot parameters

Parameter	Description	Value
T	Command update interval	20 ms
δT	Computation time required for each command update	3 ms
Y	Guidance thruster firing deadband	2% of ΔV
Attitude control		
α	Attitude error rate of convergence	0.0765 s^{-1}
m_x	Roll axis torque level	9.8 N-m
m_y	Pitch axis torque level	4.45 N-m
m_z	Yaw axis torque level	4.45 N-m
k_D	Angular rate feedback gain	0.153 s^{-1}
k_P	Angular position feedback gain	0.0117 s^{-2}
k_L	Lyapunov function parameter	1.8×10^{-3} s^{-3}
ϵ	Attitude thruster firing deadband	2×10^{-4} s^{-2}

Mission Scenario

The sequence of events for the maneuver is illustrated in Fig. 4. Alignment and initialization of the inertial navigation system is done with the spacecraft three-axis stabilized in their nominal entry attitude. After receipt of an enable command from the ground, the autopilot slews the spacecraft to align its thrust ($+x$) axis with

Table 3 Inertial navigation system error model

Parameter	RMS (1σ) value	Units
Initial position error	0.18 (x)	
	4.00 (y)	km
	5.26 (z)	
Initial velocity error	0.06 (x)	
	0.24 (y)	m/s
	0.01 (z)	
Initial attitude error	0.1 (each axis)	deg
IMU misalignment	18	arcsec
Gyro error model		
Turn-on bias repeatability	1.0	deg/h
Bias calibration error	0.10	deg/h
Time-varying bias[a]	0.05	deg/h
Scale factor error	100	ppm
Time-varying scale factor[a]	25	ppm
Scale factor asymmetry	10	ppm
Time-varying asymmetry[a]	10	ppm
Random walk	0.10	$deg/h^{1/2}$
Accelerometer error model		
Turn-on bias repeatability	500	μg
Bias calibration error	50	μg
Scale factor error	100	ppm
Scale factor asymmetry	25	ppm
Compliance (g^2)	1.0	$μg/g^2$
White noise	1.0	mm/s

[a]Modeled as first-order Gauss–Markov processes with time constants of 1 h.

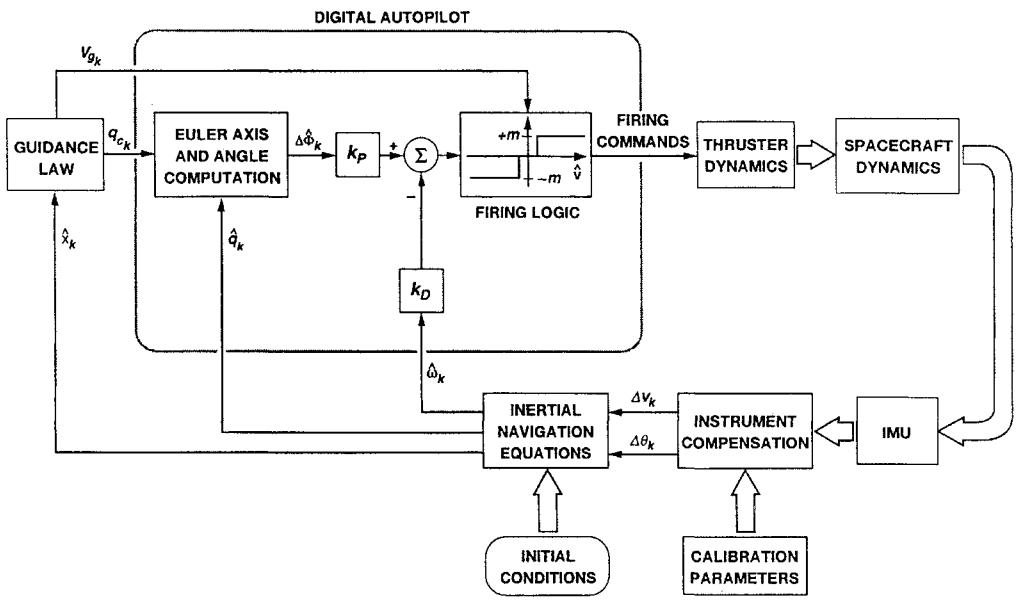

Fig. 3 Midcourse guidance system. Δv = accelerometer velocity increments (3), θ = gyro angle increments (3), $\hat{q}$ = indicated attitude quaternion, $\hat{\omega}$ = indicated angular velocity vector, $\hat{x}$ = indicated state vector (position/velocity), V_g = velocity-to-be-gained vector, q_c = commanded attitude quaternion, and $\Delta\hat{\Phi}$ = attitude error vector.

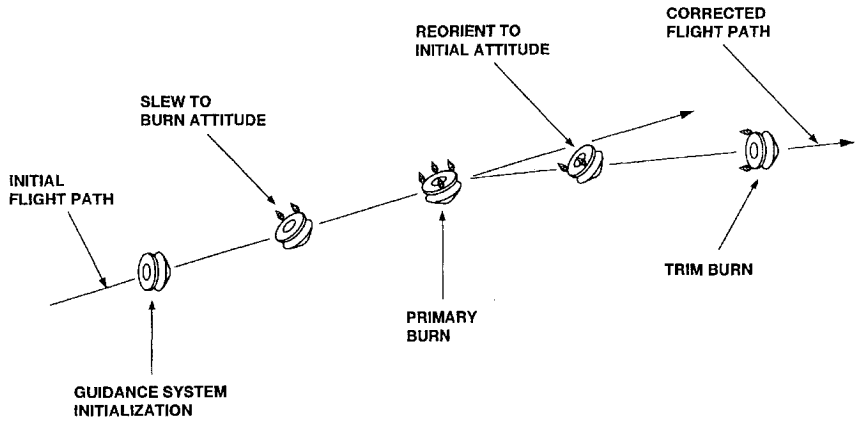

Fig. 4 Midcourse maneuver profile.

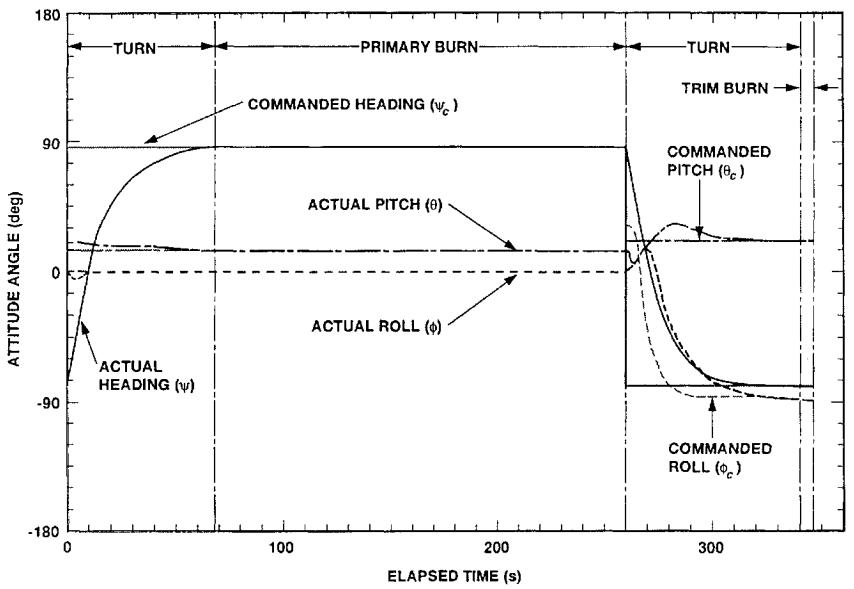

Fig. 5 Attitude angle history.

the indicated velocity-to-be-gained vector. Since the spacecraft's pitch and yaw thrusters are unbalanced, the commanded attitude changes slightly (a few degrees) during this slew maneuver, because of the change in the velocity-to-be-gained resulting from velocity changes induced by unbalanced thruster firings. Once the guidance system senses that the spacecraft has entered the limit cycle envelope about the commanded attitude, the autopilot uses the pitch and yaw thrusters to perform the commanded velocity change and to hold the spacecraft in the correct burn attitude simultaneously. Before the initiation of this burn, the velocity-to-be-gained vector computed by the guidance law is intentionally biased so that after the spacecraft returns to its initial attitude a small residual value remains, with a direction that will always have components that can be nulled by a combination of pitch/yaw and roll thruster firings.

Once the primary burn is completed, the autopilot reorients the spacecraft to its initial attitude. During reorientation, the roll angle is adjusted so that the residual velocity-to-be-gained vector lies in the plane containing the thrust axes of the roll and yaw thrusters. Finally, the autopilot performs a small trim burn while maintaining the spacecraft in its initial attitude, which nulls the residual velocity-to-be-gained induced by the velocity change of the reorientation maneuver and the bias applied to the primary burn. When firing the roll thrusters to execute velocity changes, the autopilot uses the pitch thrusters to maintain the spacecraft's attitude against the resulting disturbance torques. With this procedure, the autopilot can perform a midcourse maneuver very accurately, without the need for open-loop compensation of the translational velocity changes incurred by slewing.

Digital Computer Simulation

The flight control system was mechanized in a six-degree-of-freedom simulation, treating the spacecraft as a rigid body with variable mass and moments of inertia. No external disturbances, such as solar radiation pressure-induced torques, were modeled. The initial mass and inertia tensor were generated using a pseudo-random number generator, according to Gaussian distributions with the statistics specified in Table 1. Center of mass modeling and calibration errors were also simulated in a similar manner, with the center of mass offset statistics of Table 1 applying to both the y and z axes of the spacecraft. Thrust level variations between successive thruster firings were simulated by pseudorandom Gaussian number generation for each individual thruster. Navigation errors were simulated by numerical integration of the appropriate error equations (the interested reader is referred to the text by Britting[30]), using pseudorandom number generation to sample the statistics of the error sources described in Table 3. The time delays associated with thruster valve operation and computer operation were also simulated, using the values given in Tables 1 and 2.

Results

A simulated maneuver is shown in Figs. 5 and 6. The spacecraft must rapidly slew about 170 deg, execute a velocity change of 7.2 m/s to correct a 13-km targeting error, then return to its initial attitude. For illustrative purposes, the attitude of the spacecraft is characterized in Fig. 5 by three Euler angles; these are heading (ψ), pitch (θ), and roll (ϕ). The order of rotation for the body axes of Fig. 2 from the Mars-centered coordinate frame used by

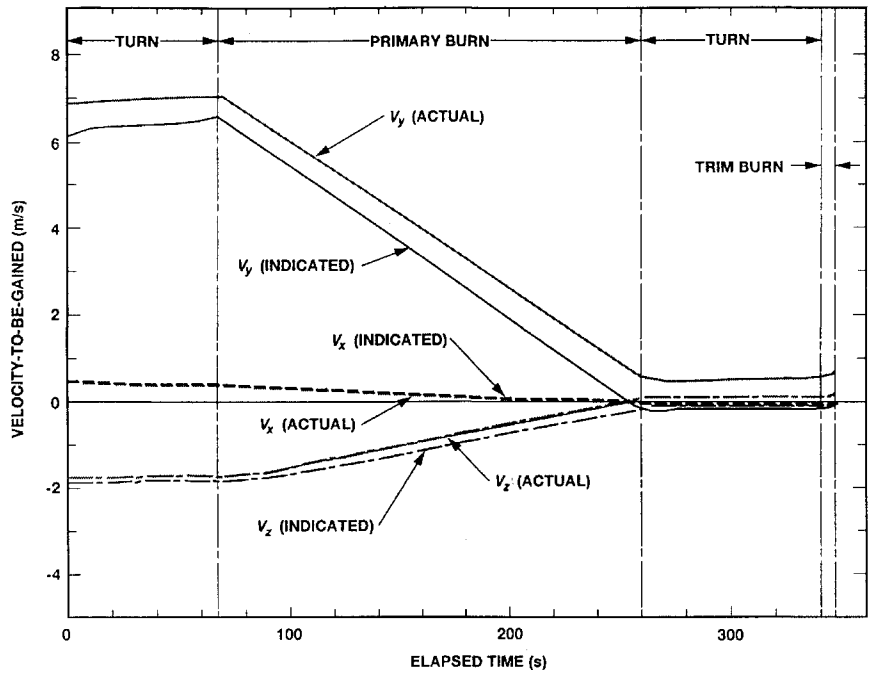

Fig. 6 Velocity-to-be-gained history.

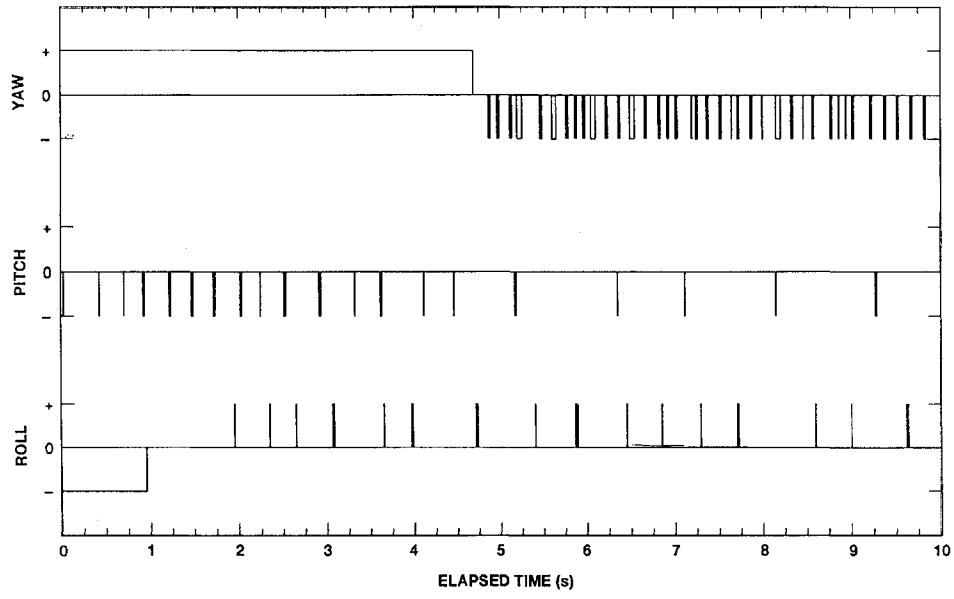

Fig. 7 Thruster firing partial history.

the navigation system to the current attitude is a rotation of angle ψ about the yaw $(+z)$ axis, followed by a rotation of angle θ about the pitch $(+y)$ axis, then a rotation of angle ϕ about the roll $(+x)$ axis. The equivalent angles representing the commanded attitude, designated ψ_c, θ_c, and ϕ_c, are also shown. There is a small limit cycle oscillation of the spacecraft about the commanded burn attitude that does not appear in Fig. 5 because of the scale used.

The actual components of the velocity-to-be-gained vector and those computed by the navigation system are shown in Fig. 6. The components of these vectors are specified in a nonrotating Mars-centered coordinate system. In this system, the x and y axes are parallel to the Martian equatorial plane, while the z axis is parallel to the mean spin axis. The flight path followed by the spacecraft during the period of interest is such that its velocity vector is oriented roughly in the $-y$ direction, inclined at an angle of about 20 deg below the equatorial $(x-y)$ plane. Differences between the actual and indicated velocity-to-be-gained components seen in Fig. 6 are because of errors in both the position and velocity vectors computed by the navigation system.

The roll, pitch, and yaw thruster firings during the first 10 s of the maneuver are shown in Fig. 7. Note that though the autopilot computes commands at a 50-Hz rate, the highest pulse frequency seen in Fig. 7 is only about 7 Hz for the yaw thrusters and 1–4 Hz for the pitch and roll thrusters, even without any low-pass filtering of the commanded torque values (such filtering may be desirable in some cases to avoid excitation of structural vibrations). As suggested by Eqs. (40) and (41), the autopilot is attempting to approximate a quasilinear system. This behavior is similar to that of the integral pulse-frequency controller of Farrenkopf et al.[2] The additional advantage possessed by the autopilot of Fig. 4 is that with pulse-width and pulse-frequency modulation, the number of thruster valve cycles during the slew maneuvers is reduced.

According to Fig. 5, the initial turn takes about 67 s to complete. In comparison, an analytical prediction of the time required to reach the commanded attitude, based on Eqs. (26), (35), and (42), was 68 s.

The primary burn takes about 190 s to complete, employing all four pitch and yaw thrusters. The attitude history of the reorientation maneuver shows that the commanded roll angle ϕ_c changes rapidly during the first 20 s. The autopilot follows this change, although reorientation takes about 80 s as opposed to 67 s for the initial turn, because of temporary saturation of the roll thrusters. Even though the commanded torque formula contains no feedforward term ($\dot{\omega}_c$), the autopilot is still able to track the commanded attitude, without the need for gain scheduling. The two slew maneuvers and the trim burn generate velocity changes with a combined magnitude of about 0.6 m/s. This represents an overhead of 8% in propellant consumption compared with the net 7.2-m/s velocity change of the maneuver. If needed, this overhead could be reduced by doing the slew maneuvers more slowly.

Conclusions

A new class of robust, exponentially convergent pulse-mode controllers for spacecraft attitude control has been developed using Lyapunov theory to predict of the behavior of a nonlinear system subject to on–off actuation. These controllers are designed to approximate a damped, quasilinear system using pulse-width and pulse-frequency modulation. The principal design parameters for a specific application are derived analytically, in terms of parameters which characterize the desired transient error convergence rate and limit cycle deadband of the complete closed-loop system. The Lyapunov function used to relate the closed-loop system behavior to the controller parameters also establishes that the desired performance is assured even in the presence of modeling errors, unmodeled disturbances, and sensor errors.

The computer simulation results illustrate the utility of the new theory for practical three-axes attitude control applications. These results suggest that excellent performance can be achieved with a relatively simple pulse-mode controller, without the need for linearizing model compensation or gain scheduling: the simulated digital autopilot was able to perform large rotational and translational maneuvers with great precision using a single set of unbalanced thrusters. Residual velocity-to-be-gained components were found to be less than 4 mm/s; this corresponds to a precision of about 0.05% in executing the simulated maneuver. The overall maneuver execution error was about 10%, due entirely to the effect of navigational errors.

Acknowledgments

The research described in this paper was carried out, in part, at the Jet Propulsion Laboratory, California Institute of Technology, under contract with NASA. The authors extend their thanks to David Spencer of Jet Propulsion Laboratory for providing Mars Pathfinder trajectory and targeting data used in the digital computer simulations.

References

[1]Gaylord, R. S., and Keller, W. N., "Attitude Control System Using Logically Controlled Pulses," *Progress in Astronautics and Rocketry*, edited by R. E. Roberson and J. S. Farrior, Vol. 8, Academic, New York, 1962, pp. 629–648.

[2]Farrenkopf, R. L., Sabroff, A. E., and Wheeler, P. C., "Integral Pulse Frequency On-Off Control," *Progress in Astronautics and Aeronautics*, edited by R. C. Langford and C. J. Mundo, Vol. 13, Academic, New York, 1964, pp. 185–230.

[3]Dahl, P. R., Aldrich, G. T., and Herman, L. K., "Limit Cycles in Reaction Jet Attitude Control Systems Subject to External Torques," *Progress in Astronautics and Rocketry*, edited by R. E. Roberson and J. S. Farrior, Vol. 8, Academic, New York, 1962, pp. 599–627.

[4]Haloulakos, V. E., "Analysis of Jet Attitude Control Systems Subject to Varying Magnitudes of External Disturbing Torques," AIAA Paper 67-537, Aug. 1967.

[5]Martin, F. H., and Battin, R. H., "Computer-Controlled Steering of the Apollo Spacecraft," *Journal of Spacecraft and Rockets*, Vol. 5, No. 4, 1968, pp. 400–407.

[6]Widnall, W. S., "Lunar Module Digital Autopilot," *Journal of Spacecraft and Rockets*, Vol. 8, No. 1, 1971, pp. 56–62.

[7]Ingoldby, R. N., "Guidance and Control System Design of the Viking Planetary Lander," *Journal of Guidance and Control*, Vol. 1, No. 3, 1978, pp. 189–196.

[8]Bergmann, E. V., Croopnick, S. R., Turkovich, J. J., and Works, C. C., "An Advanced Spacecraft Autopilot Concept," *Journal of Guidance and Control*, Vol. 2, No. 3, 1979, pp. 161–168.

[9]D'Amario, L. A., and Stubbs, G. S., "A New Single-Axis Autopilot for Rapid Spacecraft Attitude Maneuvers," *Journal of Guidance and Control*, Vol. 2, No. 4, 1979, pp. 339–346.

[10]Dwyer, T. A. W., III, "Exact Nonlinear Control of Large Angle Rotational Maneuvers," *IEEE Transactions on Automatic Control*, Vol. AC-29, No. 9, 1984, pp. 769–774.

[11]Wie, B., and Barba, P. M., "Quaternion Feedback for Spacecraft Large Angle Maneuvers," *Journal of Guidance, Control, and Dynamics*, Vol. 8, No. 3, 1985, pp. 360–365.

[12]Wie, B., Weiss, H., and Arapostathis, A., "A Quaternion Feedback Regulator for Spacecraft Eigenaxis Rotations," *Journal of Guidance, Control, and Dynamics*, Vol. 12, No. 3, 1989, pp. 375–380.

[13]Wen, J. T.-Y., and Kreutz-Delgado, K., "The Attitude Control Problem," *IEEE Transactions on Automatic Control*, Vol. AC-36, No. 10, 1991, pp. 1148–1162.

[14]Weiss, H., "Quaternion-Based Rate/Attitude Tracking System with Application to Gimbal Attitude Control," *Journal of Guidance, Control, and Dynamics*, Vol. 16, No. 4, 1993, pp. 609–616.

[15]Corless, M., "Control of Uncertain Nonlinear Systems," *Journal of Dynamic Systems, Measurement and Control*, Vol. 115, June 1993, pp. 362–372.

[16]Leitmann, G., "On One Approach to the Control of Uncertain Systems," *Journal of Dynamic Systems, Measurement, and Control*, Vol. 115, June 1993, pp. 373–380.

[17]Thurman, S. W., and Flashner, H., "New Pulse-Modulation Technique for Guidance and Control of Automated Spacecraft," *Journal of Guidance, Control, and Dynamics*, Vol. 19, No. 5, 1996, pp. 1007–1016.

[18]Utkin, V. I., *Sliding Modes and Their Application to Variable Structure Systems*, MIR, Moscow, Russia, 1978.

[19]Slotine, J. J., and Li, W., *Applied Nonlinear Control*, Prentice–Hall, Englewood Cliffs, NJ, 1991, pp. 276–307.

[20]Hughes, P. C., *Spacecraft Attitude Dynamics*, Wiley, New York, 1986.

[21]Wertz, J. R., ed., *Spacecraft Attitude Determination and Control*, D. Reidel, Dordrecht, The Netherlands, 1978.

[22]Corless, M., "Guaranteed Rates of Exponential Convergence for Uncertain Systems," *Journal of Optimization Theory and Applications*, Vol. 64, No. 3, 1990, pp. 481–494.

[23]Thurman, S. W., "A Comprehensive Guidance and Control Theory for Spacecraft Using Pulse-Modulated Propulsion," Ph.D. Dissertation, Dept. of Aerospace Engineering, Univ. of Southern California, Los Angeles, CA, Aug. 1995.

[24]Anon., "Mars Pathfinder Mission Plan," Document D-11355 Rev. A, Internal Document, Jet Propulsion Lab., California Inst. of Technology, Pasadena, CA, April 1995.

[25]Battin, R. H., *An Introduction to the Mathematics and Methods of Astrodynamics*, AIAA Education Series, AIAA, New York, 1987, pp. 550–566.

[26]Rosenberg, S. D., and Schoenman, L., "New Generation of High-Performance Engines for Spacecraft Propulsion," *Journal of Propulsion and Power*, Vol. 10, No. 1, 1994, pp. 40–46.

[27]DeLaHunt, P., Gates, S., Levenson, M., and Creamer, G., "The Clementine Attitude Determination and Control System," *Proceedings of the 8th Annual AIAA/Utah State University Conference on Small Satellites*, Logan, UT, 1994.

[28]Savage, P. G., "Strapdown Sensors," *Strapdown Inertial Systems*, NATO AGARD Lecture Series No. 95, National Technical Information Service, Springfield, VA, June 1978.

[29]Thurman, S. W., and Pollmeier, V. M., "Guidance and Navigation for the Mars Pathfinder Mission," *Acta Astronautica*, Vol. 35, Supplement, 1995, pp. 545–554.

[30]Britting, K. R., *Inertial Navigation Systems Analysis*, Wiley, New York, 1971, pp. 153–194.